JOURNAL OF PROPULSION AND POWER
Vol. 28, No. 4, July–August 2012

Aerodynamic Performance of Fan-Flow Deflectors for Jet-Noise Reduction

Juntao Xiong,* Feng Liu,† and Dimitri Papamoschou‡
University of California, Irvine, Irvine, California 92697

DOI: 10.2514/1.B34489

This paper presents a computational study on the aerodynamic effectiveness of vane-type fan-flow deflectors used for reducing jet noise from a supersonic turbofan exhaust with bypass ratio of 2.7. The numerical code solved the three-dimensional Reynolds-averaged Navier–Stokes equations. A series of nozzle configurations using deflector vanes of variable number, airfoil section, azimuthal mounting, and angle of attack are investigated. The flowfield around the vanes, overall flow turning angle, reduction of turbulent kinetic energy, thrust loss, and blockage caused by the deflector vanes are examined and characterized. Vanes using symmetric or moderately cambered airfoils cause much smaller aerodynamic losses than vanes with highly cambered sections that induce shock phenomena. Significant reduction in the turbulent kinetic energy on the underside of the jet plume can be achieved with overall flow deflection of about 1 deg and attendant specific thrust loss of 0.1%. This thrust loss is deemed small enough that a fixed-vane installation may be feasible for practical application.

Nomenclature

A = area
C_p = pressure coefficient
D_f = nozzle fan diameter
E = total internal energy
F_c = inviscid convective flux
F_d = diffusive flux
K = k-based correlator for jet noise
k = turbulent kinetic energy
$\mathcal{L}$ = lift force
M = Mach number
p = static pressure
q = dynamic pressure
$\mathcal{T}$ = thrust
u, v, w = velocity components
W = conservative variable vector
x, y, z = Cartesian coordinates
α = angle of attack
ϵ = plume deflection angle
μ_L = molecular viscosity
μ_T = turbulent viscosity
ρ = density
τ = stress tensor
ϕ = azimuth angle from downward vertical
Ω = vorticity
ω = specific dissipation rate

Subscripts

a = ambient
p = primary exhaust
s = secondary exhaust

I. Introduction

THE exhaust of jet engines continues to be a significant contributor to airport noise. The problem is particularly acute for low-bypass, high-performance turbofan engines that are envisioned to power the next generation of supersonic transports. The need for efficiency coupled with environmental compliance motivates the research and development of new nozzle concepts for supersonic aircraft, a top priority of the supersonics effort at NASA. One of these concepts, under the general category of offset-stream technologies [1], is the fan-flow deflection (FFD) method, wherein a redistribution of the fan exhaust suppresses noise from the core stream directed toward the ground. The FFD method has been the subject of past publications that focused primarily on the aeroacoustics and external velocity field [2,3]. Here, we review briefly its salient features as they relate to the present investigation, which is focused on aerodynamic performance.

The general concept of FFD is illustrated in Fig. 1. The redistribution of the fan stream can be achieved with vanes internal to the fan duct or a wedge-shaped deflector placed outside the fan nozzle. These devices act as force generators to concentrate the fan stream in the sideward and downward directions relative to the core jet, reducing velocity gradients and production of turbulent kinetic energy k in those directions. As a result, sideline and downward noise can be attenuated quite effectively, particularly in the direction of peak emission. The overall downward deflection of the plume ϵ provides an intuitive assessment of the flow turning by the vanes. It will be shown that ϵ provides guidance on the reduction in turbulent kinetic energy on the underside of the jet.

Although the link between turbulence and jet noise is very complex, the turbulent kinetic energy is a central ingredient in the formulation of models for aerodynamic noise and jet noise in particular [4]. In prevailing acoustic analogy models, the far-field intensity scales with $k^{7/2}$ ([5], for example), which underscores the significance of k in noise prediction and highlights the potential for noise reduction by decreasing k [6]. In earlier work, we examined a possible relation between the reduction in k and the reduction of the overall sound pressure level (OASPL) in the direction of peak emission [3]. The overall noise-source strength was modeled as the streamwise integral of $k_{\max}^{7/2}$, where $k_{\max}$ is the axial distribution of the maximum k in a given azimuthal direction. Denoting this integral as K, a reasonable correlation was found between the reduction of OASPL and the reduction in K. This correlation is reproduced in

Presented as Paper 2009-4212 at the 39th AIAA Fluid Dynamics Conference , San Antonio, TX, 22–25 June 2009; received 2 November 2011; revision received 23 February 2012; accepted for publication 24 February 2012.

*Postdoctoral Researcher, Department of Mechanical and Aerospace Engineering. Member AIAA.
†Professor, Department of Mechanical and Aerospace Engineering. Associate Fellow AIAA.
‡Professor, Department of Mechanical and Aerospace Engineering. Fellow AIAA.

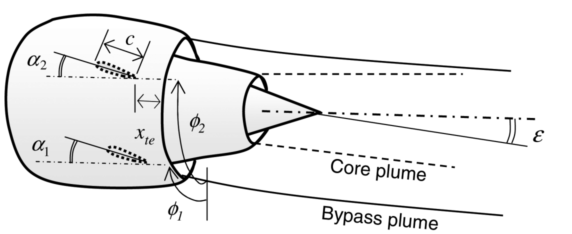

Fig. 1 Fan-flow deflection method.

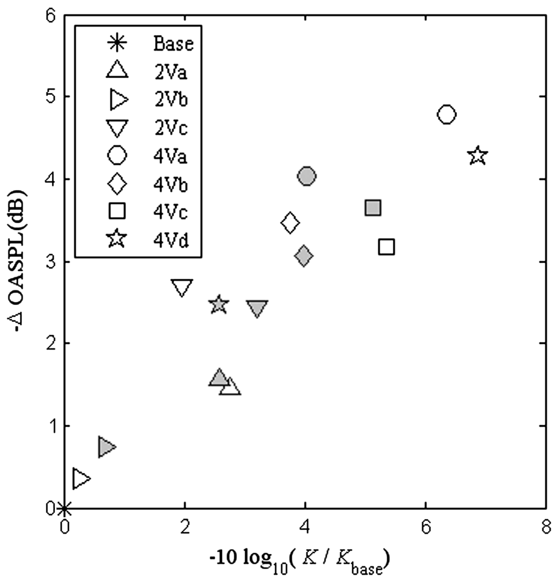

Fig. 2 Correlation of reduction in peak OASPL to reduction of integrated turbulent kinetic energy (from [3]).

Fig. 2, with K represented in decibels (note that the case labeling differs from that used in the present paper). We present this plot to illustrate the potential for noise reduction by reducing k, with the understanding that other quantities such as correlation scales have a strong impact on noise generation. We also emphasize that our use of the turbulent kinetic energy as a noise correlator is pertinent only to this particular flow and should not be construed as having general applicability to other flows. Although one cannot directly associate aircraft noise to peak OASPL, a large set of experiments have shown that a 4 dB drop in OASPL results in 3–4 dB reduction in perceived noise level [2].

The goal is therefore to provide the designer with tools for predicting the redistribution of turbulent kinetic energy, and associated aerodynamic penalty, for a given deflector configuration. The study reported here covers the aerodynamics of the complete flowfield (including the deflectors and the exhaust plume, with the goal of predicting the deflection of the fan flow), the resulting redistribution of the turbulent kinetic energy, and the thrust impact. We consider an engine cycle with bypass ratio $\mathrm{BPR} = 2.7$, appropriate for high-performance supersonic turbofan engines. We examine a variety of vane-type fan-flow deflectors with symmetric and asymmetric airfoil sections. The present study is an extension of an earlier computation on the aerodynamics of vanes for a $\mathrm{BPR} = 5.0$ nozzle that did not include the external flowfield [7]. We also note recent computational work by Dippold et al. [8] on offset-stream nozzles with $\mathrm{BPR} = 8$, including S-shaped ducts and fan-flow deflectors. Although the work we report has some similarities, our effort is focused on high-performance supersonic engines with emphasis on a detailed investigation of the aerodynamics and their connection to the redistribution of turbulent kinetic energy in the jet plume.

The computational code was first validated against experimental data on the mean velocity profiles of the jet. Thereafter it was used to simulate a series of vane configurations at engine-cycle condition to investigate aerodynamic performance and redistribution of the plume turbulent kinetic energy.

II. Computational Approach

A. Numerical Code

The computational-fluid-dynamics code used is known as PARCAE [7]. It solves the unsteady three-dimensional Reynolds-averaged Navier–Stokes (RANS) equations on structured multiblock grids using a cell-centered finite-volume method with artificial dissipation, as proposed by Jameson et al. [9]. Information exchange for flow computation on multiblock grids using multiple CPUs is implemented through the message-passing-interface protocol. The RANS equations were solved using the shear-stress transport (SST) turbulence model of Menter [10]. The SST model combines the advantages of the k–ω and k–ϵ turbulence models for both wall-bounded and freestream flows. The main elements of the code are summarized next.

The differential governing equations for the unsteady compressible flow can be expressed as follows:

$$\frac{\partial \mathbf{W}}{\partial t} + \nabla \cdot (\mathbf{F}_c - \mathbf{F}_d) = 0 \tag{1}$$

The vector $\mathbf{W}$ contains the conservative variables $(\rho, \rho u, \rho v, \rho w, \rho E)^T$. The fluxes consist of the inviscid convective fluxes $\mathbf{F}_c$, and the diffusive fluxes $\mathbf{F}_d$ are defined as

$$\mathbf{F}_c = \begin{Bmatrix} \rho u & \rho v & \rho w \\ \rho uu + p & \rho uv & \rho uw \\ \rho vu & \rho vv + p & \rho vw \\ \rho wu & \rho wv & \rho ww + p \\ \rho Eu + pu & \rho Ev + pv & \rho Ew + pw \end{Bmatrix} \tag{2}$$

$$\mathbf{F}_d = \begin{Bmatrix} 0 & 0 & 0 \\ \tau_{xx} & \tau_{xy} & \tau_{xz} \\ \tau_{yx} & \tau_{yy} & \tau_{yz} \\ \tau_{zx} & \tau_{zy} & \tau_{zz} \\ \Theta_x & \Theta_y & \Theta_z \end{Bmatrix} \tag{3}$$

with

$$\mathbf{\Theta} = \mathbf{u}\colon \boldsymbol{\tau} - \left(\frac{\mu_L}{Pr_L} + \frac{\mu_T}{Pr_T}\right)\nabla T \tag{4}$$

The stress tensor $\boldsymbol{\tau}$ depends on the viscosity $\mu = \mu_L + \mu_T$, where the subscripts L and T represent laminar and turbulent contributions, respectively. Pr_L and Pr_T are the laminar and turbulent Prandtl numbers, respectively.

The closure model used to evaluate the turbulent viscosity μ_T is the k–ω SST turbulence model, given by the following equations:

$$\begin{aligned} \frac{\partial \rho k}{\partial t} + \nabla \cdot (\rho k \mathbf{u} - \mu_k^* \nabla k) &= \rho S_k \\ \frac{\partial \rho \omega}{\partial t} + \nabla \cdot (\rho \omega \mathbf{u} - \mu_\omega^* \nabla \omega) &= \rho S_\omega \end{aligned} \tag{5}$$

where $\mu_k^* = \mu_L + \sigma_k \mu_T$, $\mu_\omega^* = \mu_L + \sigma_\omega \mu_T$, and $\mu_T = (\rho a_1 k)/\max(a_1 \omega; \Omega f_2)$. The source terms S_k and S_ω are

$$S_k = \frac{1}{\rho} \boldsymbol{\tau}\colon \nabla \mathbf{u} - \beta^* \omega k$$

$$S_\omega = \frac{\gamma}{\mu_\tau} \boldsymbol{\tau}\colon \nabla \mathbf{u} - \beta \omega^2 + 2(1 - f_1) \frac{1}{\omega} \nabla k \cdot \nabla \omega$$

In the previous equations, f_1 and f_2 are blending functions; and the parameters a_1, σ_k, σ_ω, β, β^*, and γ are closure coefficients.

The flow and turbulence equations are discretized in space by a structured hexahedral grid using a cell-centered finite-volume

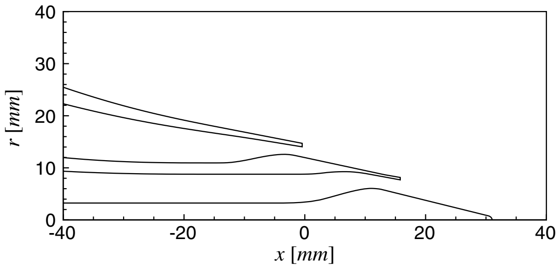

Fig. 3 Coordinates of the bypass ratio BPR = 2.7 (B27) nozzle.

method. Because each block is considered as a single entity within the code, only flow and turbulence quantities at the block boundaries need to be exchanged. The governing equations are solved explicitly in a coupled manner through a five stage Runge–Kutta scheme toward the steady state with local time stepping, residual smoothing, and multigrid for convergence acceleration. Unlike previous computational studies of fan-flow-deflected nozzle flow [8], a low-speed preconditioner [11] is employed to simulate low ambient Mach number of the nozzle and jet plume flows. Further details of the numerical method can be found in [3].

B. Computational Model and Grid

The computations were performed on a dual-stream turbofan nozzle with bypass ratio BPR = 2.7 (B27 nozzle), used in past subscale experimental investigations [2]. The radial coordinates are plotted in Fig. 3 The fan exit diameter is $D_f = 28.1$ mm, and the fan exit height is 1.8 mm. Details of the thermodynamic cycle of the B27 nozzle can be found in [2]. Deflection of the fan stream was achieved by the use of internal airfoil-shaped vanes. Configurations consisting of single (2V) and twin (4V) pairs of vanes with NACA0012, NACA4412, and NACA7514 airfoil sections were studied. The vanes were placed at various azimuth angles and angles of attack. For all the cases reported here, the vane chord length was 3.0 mm and the vane trailing edge was situated 2.0 mm upstream of the fan exit plane. Table 1 lists the details of the nozzle configurations and includes aerodynamic performance parameters to be discussed in Sec. III. Figure 1 illustrates the vane parameters.

Multiblock grids were generated for each vane configuration. Because all of the vane configurations were symmetric to the meridional plane, only one half (180 deg) of the nozzle was modeled to save computation cost. To simulate the jet flow, the grids extended to $3.8D_f$ radially outward from the nozzle centerline and over $20D_f$ downstream of the nozzle. A *C* grid surrounded each vane in the region near the exit plane to capture the features of boundary-layer and wake flows accurately. The outer-region grids for all cases were kept the same to simplify grid-generation work. A patch-connection interpolation technique [12] was used to transfer flow-variable information between nonmatching connection surfaces. Figure 4 shows a detail of the grid for the 4Ve nozzle. The grids were clustered all along the wall boundaries. The base nozzle grid had 3.7 million grid points. The 2V and 4V configurations had 4.9 million and 5.8 million grid points, respectively. For all the grids, the minimum y^+ of the first grid point from the wall was less than 1. The average y^+ values were about 3. Wall functions were not required. The grids were divided into multiblock to implement parallelization on multiprocessors computers to reduce computational time.

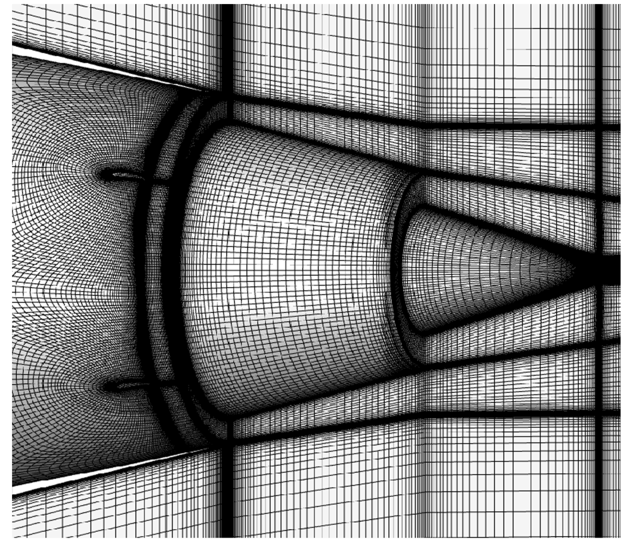

Fig. 4 Detail of computational grid for 4Ve nozzle.

We conducted two sensitivity studies, the first to test grid independence and the second to assess the effect of the small forward velocity on the computational results. Grid independence was evaluated by reducing the number of grid points by 50% (21% in each spatial direction). The effect of the 17 m/s ambient velocity was evaluated by augmenting the core and fan velocities (cold conditions) by 17 m/s, thus maintaining the same velocity differences between jet flows and ambient as in the experiments. Both changes produced minute (less than 2%) changes on the velocity and turbulent kinetic energy fields, thus indicating adequate grid resolution and minimal impact of the forward velocity on the results. Further details on the grid-sensitivity study for this flowfield can be found in [3].

C. Flow and Boundary Conditions

The flow conditions in the computations simulated those in subscale experiments conducted in our facilities. Experiments were conducted at the two set points shown in Table 2. The hot set point reflects the engine cycle for the B27 nozzle and was used in acoustic tests; the cold condition was used in the mean velocity surveys. The hot and cold conditions share the same velocity ratio and the same primary exit Mach number. All the experimental tests were static. The jet Reynolds numbers for the hot and cold conditions were 0.92×10^6 and 0.47×10^6, respectively, based on the exit diameter of the fan nozzle and the secondary exit conditions. The larger

Table 1 Nozzle configurations and aerodynamic performance parameters

Nozzle	Airfoil[a]	α_1, deg	ϕ_1, deg	α_2, deg	ϕ_2, deg	$\Delta\dot{m}$, %	ΔT, %	ϵ, deg	$K_{\phi=0\ \mathrm{deg}}$	$K_{\phi=60\ \mathrm{deg}}$	$K_{\phi=180\ \mathrm{deg}}$
Base						0.000	0.000	0.000	1.633	1.633	1.633
2Va	0012	7.5	90			0.036	0.076	0.584	0.864	0.909	2.300
2Vb	0012	7.5	150			0.035	0.072	0.295	1.540	1.392	3.139
2Vc	7514	4.0	120			0.121	0.224	0.692	1.042	0.785	3.801
4Va	0012	0.0	50	0.0	120	0.005	0.047	0.000	1.710	1.605	1.705
4Vb	0012	7.5	50	7.5	120	0.085	0.153	0.941	0.514	0.896	3.085
4Vc	0012	10.0	50	10.0	120	0.217	0.321	1.242	0.404	0.690	3.366
4Vd	0012	7.5	90	7.5	150	0.083	0.419	0.815	0.692	0.649	3.984
4Ve	7514	4.0	50	4.0	120	0.560	0.721	1.351	0.378	0.652	3.382
4Vf	7514	4.0	50	4.0	90	0.556	0.715	1.453	0.335	0.854	2.045
4Vg	4412	7.5	90	4.0	150	0.182	0.262	1.168	0.476	0.506	4.346

[a]NACA section.

Table 2 Exhaust conditions

Property	Hot (cycle point)	Cold
U_p, m/s	600	319
M_p	1.03	1.03
U_s, m/s	400	213
M_s	1.15	0.65
A_s/A_p	1.40	1.40
U_s/U_p	0.67	0.67

Reynolds number of the hot cycle point is due to the higher secondary Mach number.

The computation captured these conditions, with the exception that a small forward Mach number $M_a = 0.05$ was used for numerical stability. Computations at the cold set point were used for validation against the experimental mean velocity field. The hot set point was used for the investigation of aerodynamic performance. Uniform total pressure, uniform total temperature, and zero-flow angle were specified at the inlet surface for both the fan and core duct flows. For the ambient region surrounding the nozzle flow, a characteristic boundary condition was defined, and the downstream static pressure was set to the ambient pressure. The adiabatic no-slip boundary condition was specified on all the nozzle and vane solid walls.

D. Aerodynamic Parameters

The force generated by the jet was evaluated using a control volume that surrounded the entire nozzle. The thrust force results from integration of the axial momentum and pressure on the exit surface A of the control volume, located $0.5D_s$ downstream of the plug tip:

$$\mathcal{T} = \int_A (\rho u^2 + p - p_a)\,\mathrm{d}A \tag{6}$$

The overall lift force of the jet involves integration of the transverse momentum flux on the exit of the control volume:

$$\mathcal{L} = \int_A \rho v u\,\mathrm{d}A \tag{7}$$

The mass flow rate was obtained by integration of the mass flux on the fan and core nozzle exit surfaces:

$$\dot{m} = \int_{A_{p+s}} \rho u\,\mathrm{d}A \tag{8}$$

The specific thrust is defined as

$$\mathcal{T}_s = \frac{\mathcal{T}}{\dot{m}} \tag{9}$$

Assuming small angles, the overall deflection of the plume is

$$\epsilon = \frac{\mathcal{L}}{\mathcal{T}} \tag{10}$$

The losses in mass flow rate, thrust, and specific thrust are defined by the following equations:

$$\Delta\dot{m} = \dot{m}_{\mathrm{clean}} - \dot{m} \tag{11}$$

$$\Delta\mathcal{T} = \mathcal{T}_{\mathrm{clean}} - \mathcal{T} \tag{12}$$

$$\Delta\mathcal{T}_s = \mathcal{T}_{\mathrm{sclean}} - \mathcal{T}_s \tag{13}$$

where the subscript "clean" refers to the nozzle without vanes. Note that losses are defined to be positive.

The vane airfoils are situated in an accelerating freestream due to the convergence of the duct walls. Definition of the aerodynamic coefficients becomes problematic, as there is no fixed reference condition. Here, we use as reference the area-averaged conditions in the plane of the vane leading edge (LE) in the absence of the vane. The pressure coefficient is thus defined as

$$C_p = \frac{p - p_{\mathrm{LE}}}{q_{\mathrm{LE}}} \tag{14}$$

III. Results and Discussion

The computations were first validated with experimental measurements of the mean velocity field at the cold condition. Then, the code was extended to the hot condition to investigate the impact on nozzle aerodynamic performance of the fan-flow deflector.

A. Validation Against Mean Flow Measurement

The computational code was validated by comparing the computed axial velocity of the jet to experimental measurements. The results for the baseline and 4Ve nozzles are shown in Figs. 5 and 6, respectively. The mean velocity fields are presented in the forms of isocontours on the symmetry plane, isocontours on several transverse planes, and line plots on the symmetry plane at several axial locations. Considering the baseline nozzle, the results on the symmetry plane indicate a good match of the potential core length and of the growth rate. The transverse plots also show good agreement except in very close to the nozzle, where the computed wake from the plug is more pronounced than in the experimental data. The computation indicates that the wake region is very thin; it is thus probable that the finite spatial resolution of the experimental measurement, defined by the probe diameter, smoothed out the details of the wake region. It is also possible that the k–ω SST model underestimates mixing in the wake region. Examining now the 4Ve in Fig. 6, the computation captures the thickening of the fan stream on the underside of the core jet and the distortion of the transverse profiles from circular to oval. More details of these and other validation data can be found in [3]. The close agreement with experiment provides us with confidence in applying the code for the study of aerodynamic performance.

B. Flowfield Around the Deflector Vanes

We study the flowfield around the deflector vanes to gain insight into the detailed aerodynamics of the flow turning and their dependence on airfoil section, angle of attack, and azimuthal position. For brevity, we confine our discussion to the 4V configurations listed in Table 1. Figures 7–12 show the computed Mach number contours and the pressure distributions at the midspan section of the deflector vanes for five of the 4V configurations. The C_p^* line marks the critical pressure coefficient where the flow becomes sonic.

The first three configurations use two pairs of NACA0012 airfoils mounted at $\phi_1 = 50$ deg and $\phi_2 = 120$ deg. The angles of attack are 0, 7.5, and 10 deg for the 4Va, 4Vb, and 4Vc configurations, respectively. The accelerating freestream, due to the convergence of the nozzle walls, is evident in the Mach-number and pressure distributions of Figs. 7–9. The acceleration produces thin boundary layers and wakes, which minimizes blockage compared to the case of an open freestream. As the angle of attack increases, the Mach contours and the surface pressure distribution reveal a sharp suction peak at the leading edge of the airfoil followed by a strong pressure diffusion behind the peak, which thickens the boundary layer and therefore results in increased drag. In addition, this suction peak may cause a supersonic pocket with a possible shock wave at higher angles of attack. Both the shock wave and possible shock-induced separation would cause losses and blockage and therefore should be avoided. At 10 deg angle of attack, the 4Vc case shows a small supersonic bubble near the leading edge. Changing the azimuth angles to $\phi_1 = 90$ deg and $\phi_2 = 150$ deg resulted in very minor differences in the vane flowfields discussed previously.

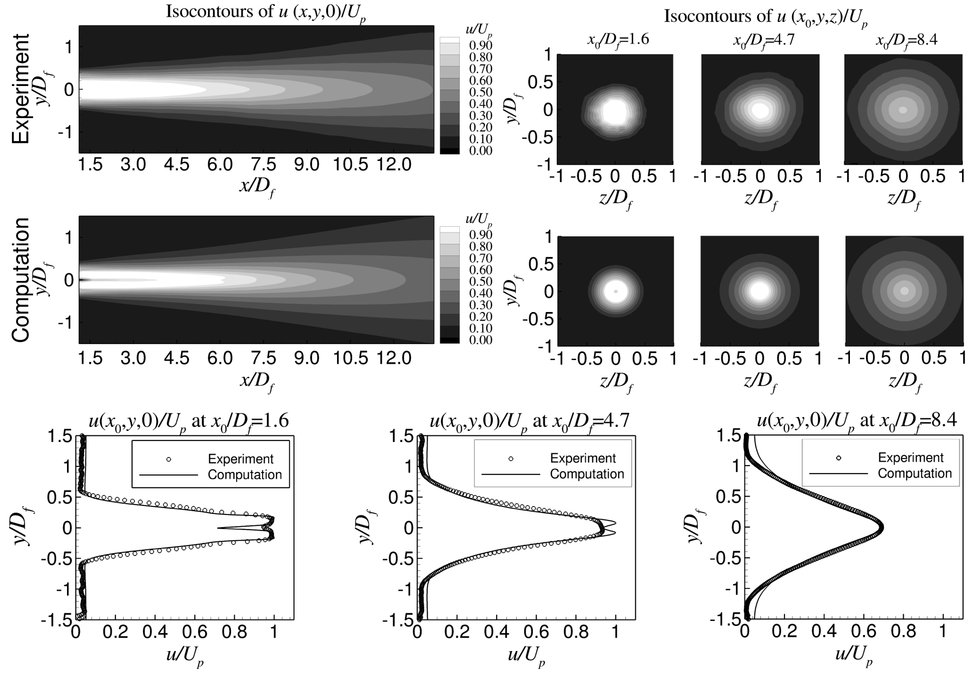

Fig. 5 Comparison of computational and experimental mean velocity fields for the baseline nozzle.

Figures 10 and 11 examine the effects of using the cambered NACA7514 airfoil instead of symmetric NACA0012 airfoil. For the 4Ve case, the azimuthal mounting positions are the same as those for the first three 4V cases. Because the airfoil is cambered, a smaller angle of attack (4 deg) is set for this configuration. Despite the small angle of attack, both the Mach contours and the surface pressure distribution show a large supersonic pocket with a strong terminating shock wave on the back of the airfoil. The camber overloads the rear portion of the airfoil, resulting in a large suction area in the accelerating freestream. Reducing the azimuthal separation of the vanes in case 4Vf (Fig. 11) appears to somewhat enhance the high-Mach-number environment near the nozzle exit.

Figure 12 examines the 4Vg configuration, where the NACA7514 airfoil is replaced by the less-cambered and thinner NACA4412 airfoil. The dissimilar angles of attack in this case cause an obvious difference in the loading of the upper and lower vane pairs. The mounting azimuth angles are the same as those for the 4Vd configuration. The decreased camber and thickness reduce the suction peaks compared to those on the NACA7514 airfoil. However, the rear part of the bottom vanes remains slightly overloaded.

C. Pressure Field on Core Cowl

A distinct aspect of the present study over a previous investigation [7] is the resolution of the entire internal and external nozzle flow, which includes the core cowl. Examination of the pressure distribution on the core cowl is important for identifying any thrust impacts from the pressure field of the deflectors in conjunction with the slope of the cowl. To present a map of the pressure distribution of

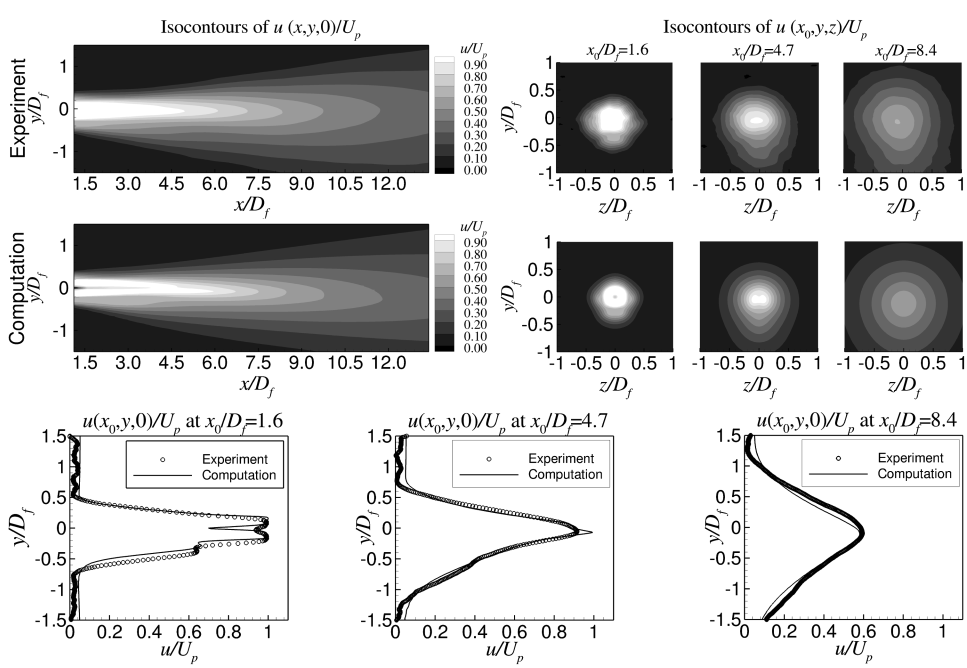

Fig. 6 Comparison of computational and experimental mean velocity fields for the 4Ve nozzle.

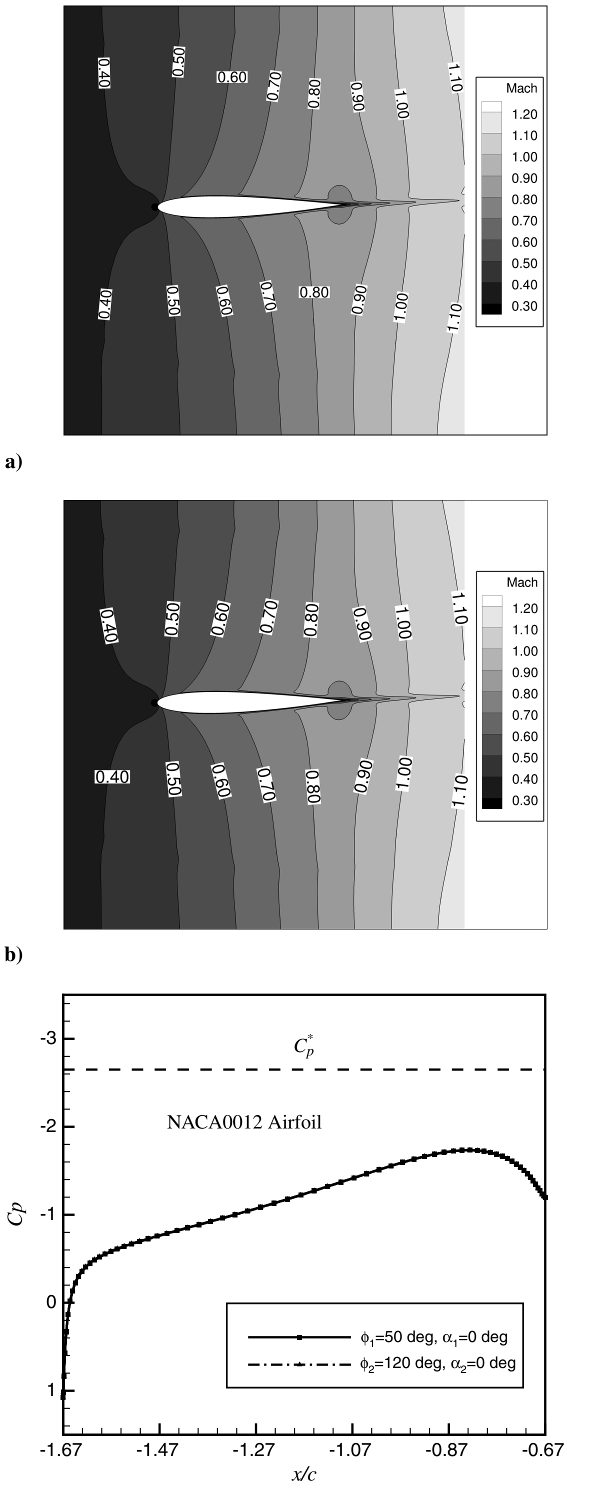

Fig. 7 Internal aerodynamics of 4Va fan nozzle: a) Mach number contours for upper pair of vanes, b) Mach number contours for lower pair of vanes, and c) surface pressure distribution on midplane of vane.

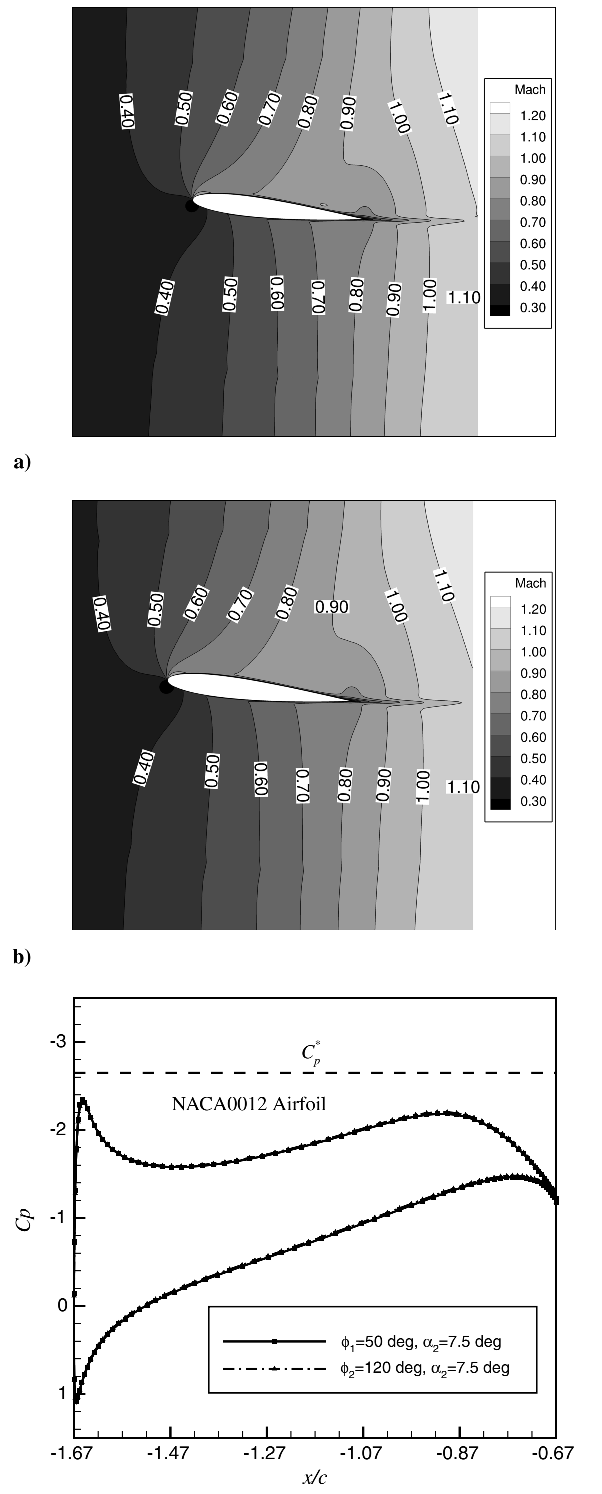

Fig. 8 Internal aerodynamics of 4Vb fan nozzle: a) Mach number contours for upper pair of vanes, b) Mach number contours for lower pair of vanes, and c) surface pressure distribution on midplane of vane.

the cowl, we unfold the cowl and plot this distribution versus x and ϕ. Figure 13 displays such a plot for the differential pressure between case 4Vf and the baseline. The location of the vanes is shown for clarity. Prominent on the figure are two high-pressure regions that follow the suction side of each vane. This compression appears to be due to pressure recovery after the suction.

We obtain more quantitative information by plotting the circumferentially averaged differential pressure in Fig. 14. We observe that the vanes create an overall compression on the core cowl. Integrated over axial distance, this compression results in a small but important contribution to thrust. The next section will discuss further this contribution.

D. Aerodynamic Performance

Table 1 summarizes the aerodynamic results for all the configurations studied, together with turbulent kinetic energy predictions to be discussed in the next subsection. The 2V cases

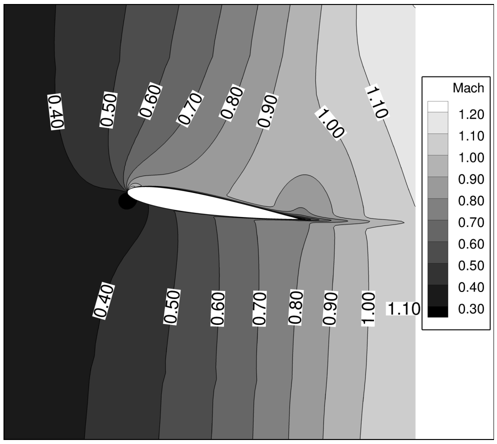

a)

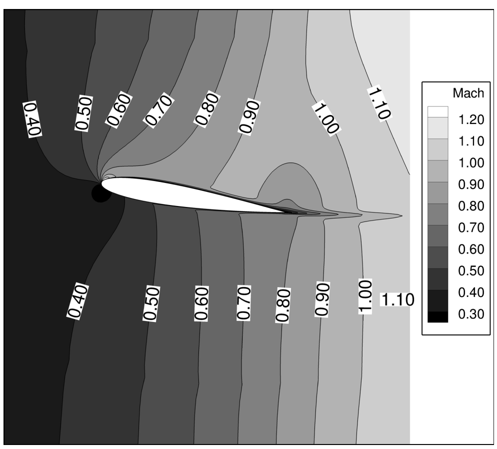

b)

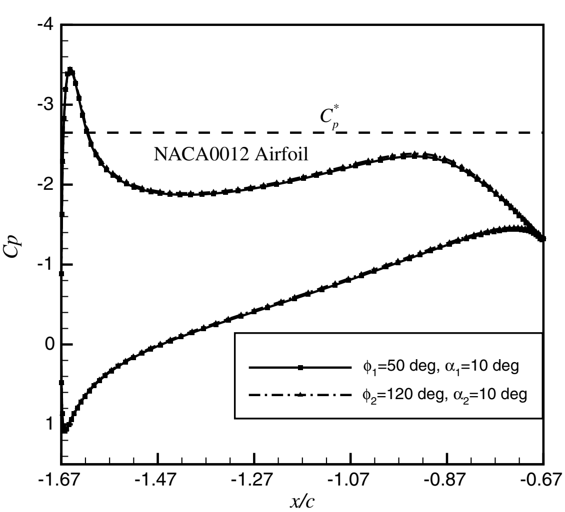

c)

Fig. 9 Internal aerodynamics of 4Vc fan nozzle: a) Mach number contours for upper pair of vanes, b) Mach number contours for lower pair of vanes, and c) surface pressure distribution on midplane of vane.

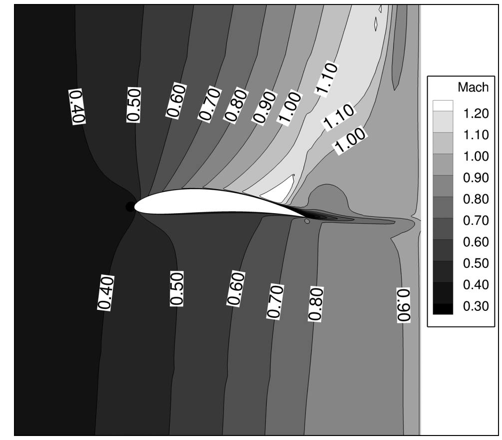

a)

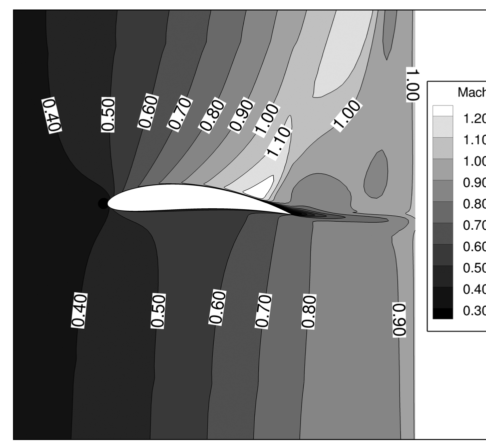

b)

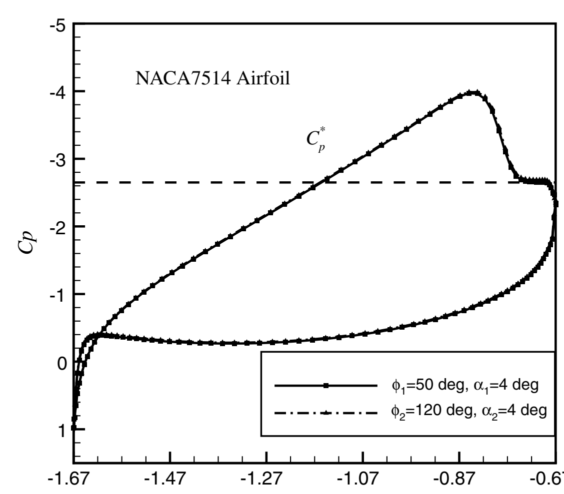

c)

Fig. 10 Internal aerodynamics of 4Ve fan nozzle: a) Mach number contours for upper pair of vanes, b) Mach number contours for lower pair of vanes, and c) surface pressure distribution on midplane of vane.

cause moderate plume deflection, up to 0.69 deg for case 2Vc. Setting the vanes to high azimuth angle, case 4Vb, naturally reduces the downward deflection, although such arrangements may be beneficial for thickening the fan flow in the sideline direction.

Larger deflections are enabled with the 4V configurations, with the NACA7514 vanes proving the most effective in turning the flow. However, as pointed out earlier, the highly cambered airfoils induce strong shock phenomena, which are responsible for the significant blockage and thrust loss listed in Table 1 for cases 4Ve and 4Vf. The nozzles with symmetric (NACA0012) or moderately cambered (NACA4412) airfoils provide adequate deflections with small losses. Naturally, increasing the angle of attack increases the plume deflection, as evidenced by nozzles 4Vb and 4Vc. Comparing nozzles 4Vb and 4Vd, and nozzles 4Ve and 4Vf,, we note that the azimuthal placement has a moderate impact on the downward plume deflection, The 4V nozzles include vanes with zero lift, case 4Va, which provides a reference point for the losses when the vanes are deactivated.

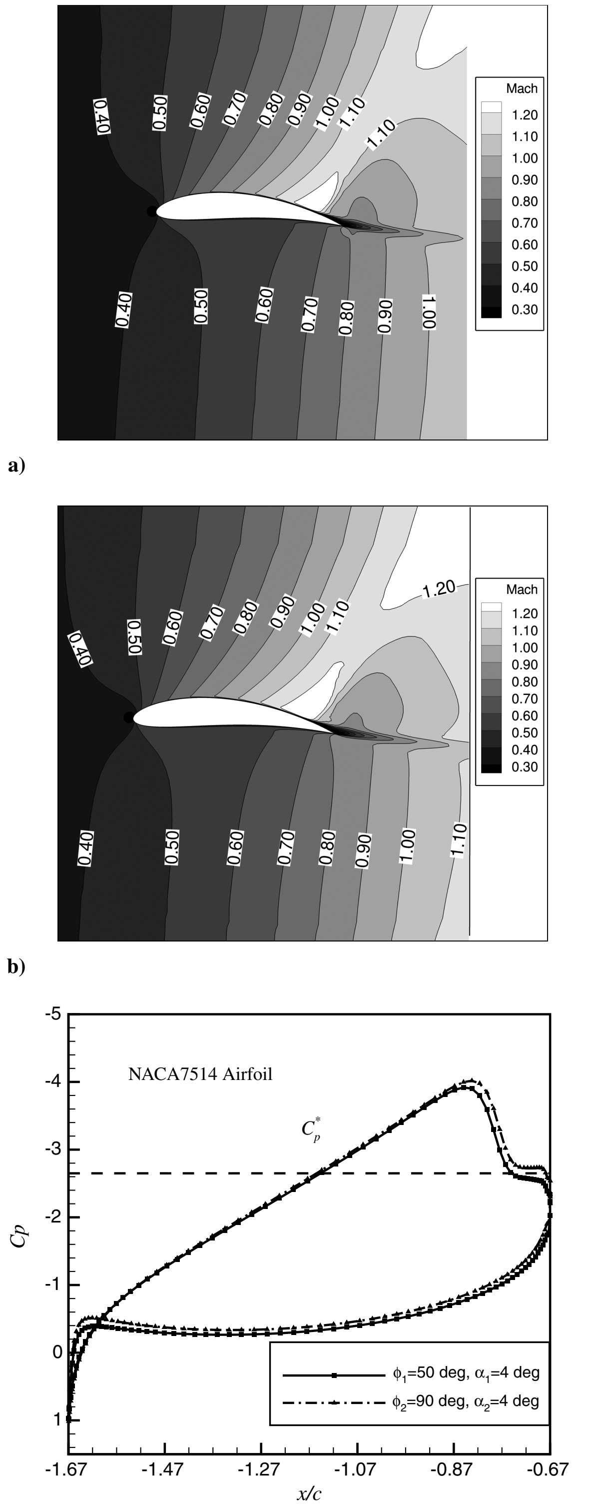

Fig. 11 Internal aerodynamics of 4Vf fan nozzle: a) Mach number contours for upper pair of vanes, b) Mach number contours for lower pair of vanes, and c) surface pressure distribution on midplane of vane.

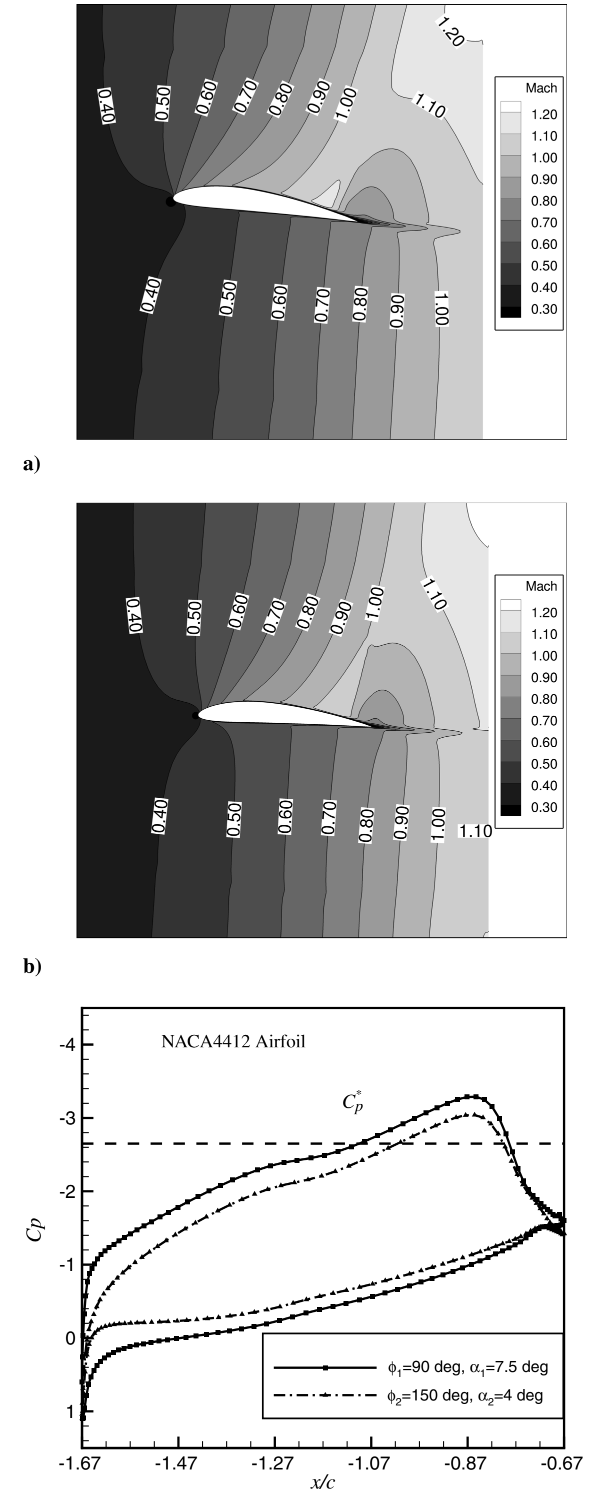

Fig. 12 Internal aerodynamics of 4Vg fan nozzle: a) Mach number contours for upper pair of vanes, b) Mach number contours for lower pair of vanes, and c) surface pressure distribution on midplane of vane.

The aerodynamic performance is best understood by plotting the losses in thrust and mass flow rate versus the plume deflection angle. We stress that the results presented are for the entire nozzle. Figure 15 shows these relationships. The NACA0012 vanes cause a thrust loss of 0.05% at $\epsilon = 0$ deg rising to 0.35% at $\epsilon = 1.2$ deg. Near this deflection angle, the thrust loss caused by the NACA4412 vanes is similar to that caused by the NACA0012 vanes. However, the highly cambered NACA7514 vanes cause substantial thrust loss approaching 0.75% at large deflection angle. We note that a large fraction of the thrust loss at large deflection angle is due to mass-flow loss, or blockage, induced by the vanes. It is thus informative to examine the specific thrust loss, plotted in Fig. 16. For the NACA0012 deflectors, the specific thrust loss ranges from 0.042% at $\epsilon = 0$ deg to 0.104% at $\epsilon = 1.2$ deg. The NACA4412 vanes have slightly better performance than the NACA0012 vanes at $\epsilon = 1.2$ deg. In contrast, the NACA7514 vanes cause substantially higher loss due to the strong shock wave occurring in the rear part of the vanes.

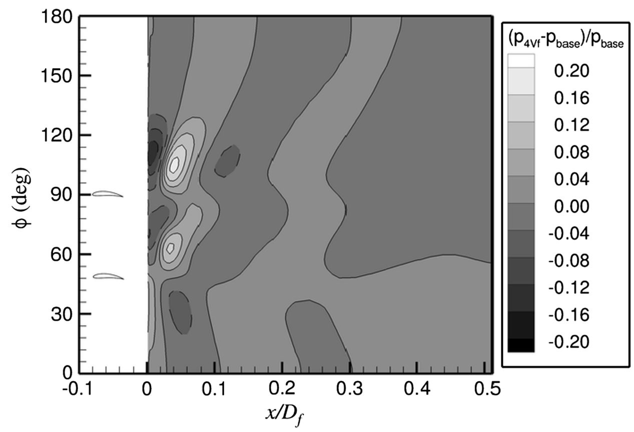

Fig. 13 Differential pressure distribution on core cowl for case 4Vf.

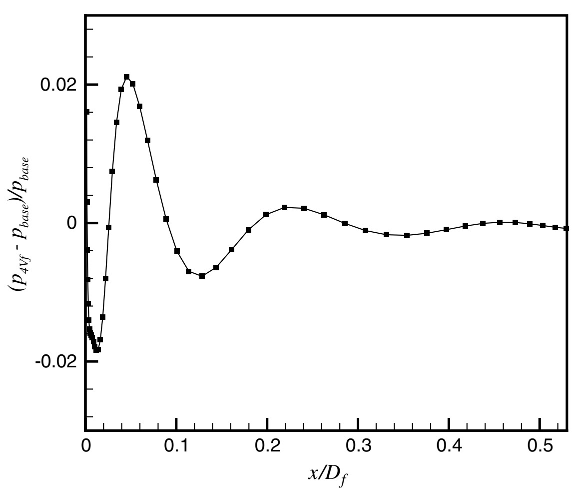

Fig. 14 Circumferentially averaged differential pressure distribution on core cowl for case 4Vf.

To quantify the impact of the core cowl on aerodynamic performance, Fig. 16b plots the specific thrust loss obtained by integration of the axial momentum and pressure on the core and fan nozzle exit surfaces, thus omitting the contribution of the cowl. Without accounting for the cowl, the specific thrust loss is higher by as much as 16%. In other words, if the core cowl is not included in the thrust calculation, one overestimates the thrust loss caused by the deflectors. This underscores the beneficial thrust contribution of the cowl when the deflectors are installed, as discussed previously in Sec. III.C.

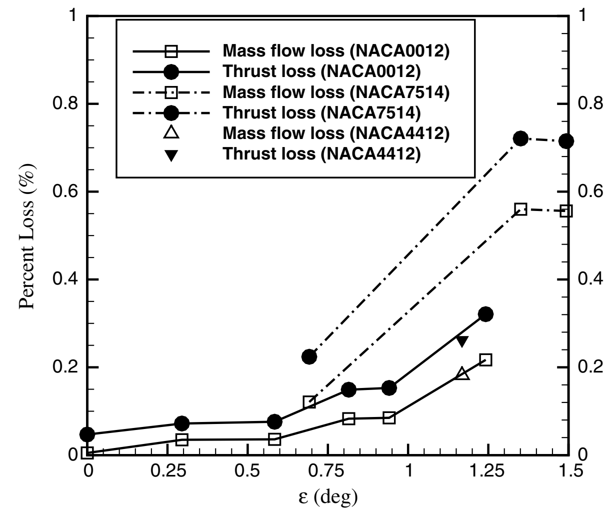

Fig. 15 Losses of mass flux and thrust vs plume deflection angle.

In the practical implementation of the vane deflection approach, the designer is faced with the choice whether to configure the vanes for fixed or variable angle of attack. As shown in Fig. 16a, the variable incidence would reduce the specific thrust loss from 0.1% with the vanes activated to 0.04% for the vanes deactivated (set to zero lift). The marginal benefit of only 0.06% may not justify the complexity and weight of an actuation mechanism. Because the specific thrust loss is very small even at the large plume deflection angle of 1.2 deg, the designer may opt to have the vanes fixed, accounting for the vane blockage by expanding the fan exit area. Of course, a thrust analysis would also be needed for the cruise condition. Although we have not conducted this analysis, we note that, at supersonic cruise, a large fraction of the thrust comes from the core stream, which is unaffected by the FFD scheme. It is thus likely that the thrust loss will be of the same order as on takeoff.

E. Impacts on Turbulent Kinetic Energy

As discussed in Sec. I, an important fluid–dynamical role of the deflectors is to redistribute the turbulent kinetic energy k field in the jet plume. We examine this redistribution and correlate it to the plume deflection angle. First, we look at contour maps of k on the symmetry

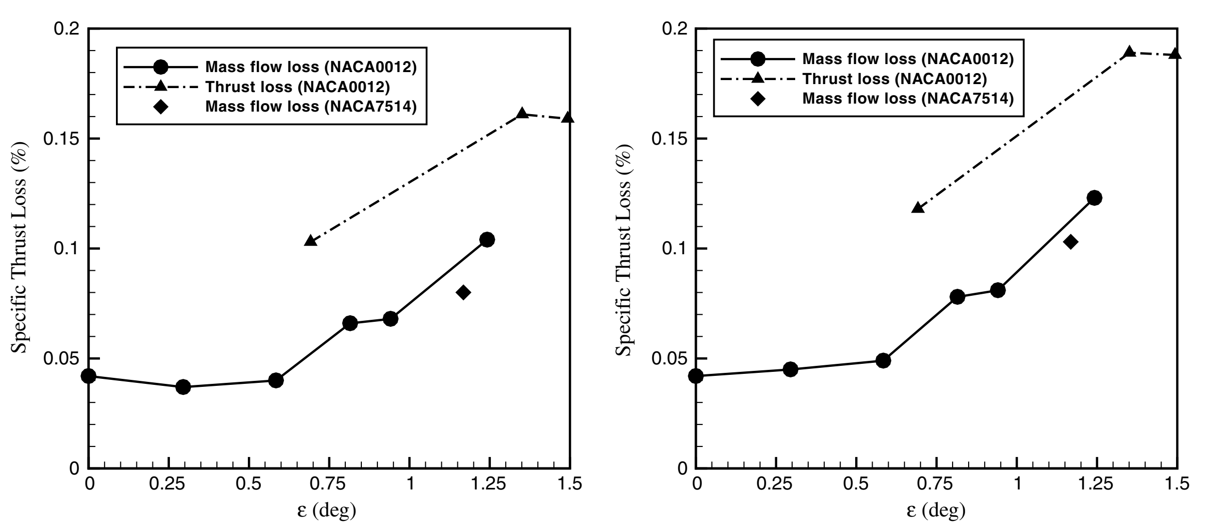

Fig. 16 Specific thrust loss vs plume deflection angle a) based on control volume surrounding entire nozzle, and b) based on integration at the exit planes of the fan and core nozzles (without core cowl contribution).

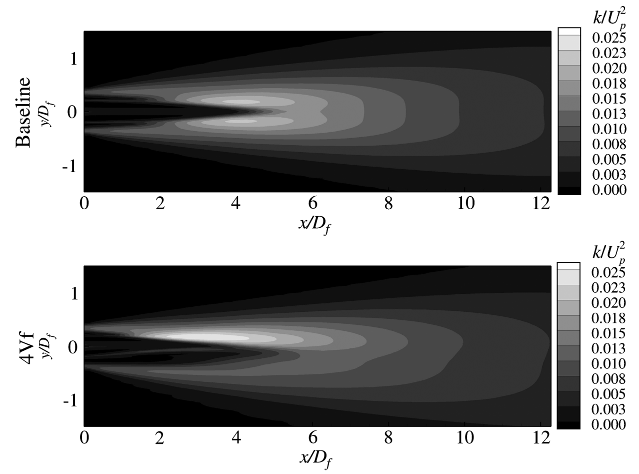

Fig. 17 Distribution of turbulent kinetic energy on the symmetry plane for the baseline and 4Vf nozzles.

plane. Figure 17 compares the k fields for the baseline and 4Vf nozzles. We note a decrease in k on the lower side of the jet with an accompanying increase on the upper side. The trends observed in Fig. 17 are similar to those seen in computational and experimental studies of fan-flow deflectors in larger-bypass nozzles [8]. For deflection angles around 1.2 deg, the peak level of k is reduced by approximately 50% on the underside of the jet.

Based on the results exemplified in Fig. 17, we compute the axial integral $K = \int k_{\max}^{7/2}\,\mathrm{d}x$, where $k_{\max}(x)$ is the maximum level of k in a particular azimuthal direction. Recall that the reduction of K was used as a correlator for the reduction in OASPL (Fig. 2). The values of K in the downward ($\phi = 0$ deg), sideline ($\phi = 60$ deg), and upward ($\phi = 180$ deg) directions are listed in Table 1. We note that the 4V configurations generally lead to a substantial reduction of K, of about 70%, in the downward and sideline reductions. However, in cases with very strong downward deflections, the substantial reduction in downward K comes at a cost of moderate reduction in sideline K. This calls for a balanced approach when the noise at all the certification points is considered. In all cases, there is an increase of K at the top of the jet. This increase is not expected to impact the directive component of jet noise associated with large-scale structures emitting in the downward direction but may impact other, weaker components that impact the large angles from the jet axis. Again, this calls for a balanced approach in the implementation of the vanes.

To summarize the key trends in the downward direction, we plot the reduction of downward K, expressed in the logarithmic form of

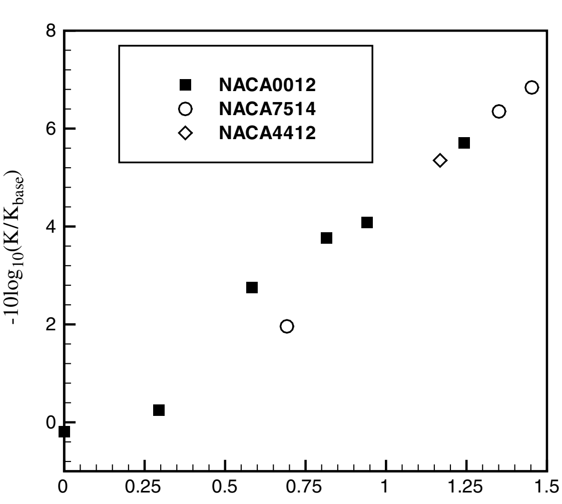

Fig. 18 Reduction in downward integrated turbulent kinetic energy K vs plume deflection angle.

decibels, versus plume defection angle in Fig. 18. We note that all the vane configurations collapse practically on a single trend of K reduction with increasing plume deflection angle. The figure shows a very small increase in K at $\epsilon = 0$ deg, the result of the vane wakes of configuration 4Va. The correlation of Fig. 18 indicates that the overall plume deflection angle is a good indicator of noise reduction in peak OASPL, at least for the downward direction. Combining the results of Figs. 2 and 18, a plume deflection of 1.2 deg has the potential to yield an OASPL reduction of 4 dB. Although the overall noise reduction is more complex than that described by the peak OASPL, this trend gives useful guidance to the designer as to the overall deflection required to attain a given noise reduction goal.

IV. Conclusions

We presented a computational study on the aerodynamic effectiveness of vane-type fan-flow deflectors in redistributing the turbulent kinetic energy in the plume of a supersonic turbofan exhaust with bypass ratio 2.7. We examined vanes of varying cross sections, angles of attack, and azimuthal mounting positions. The computational code was validated against experimental measurement of the mean velocity field of the jet. Our investigation focused on the internal aerodynamics of the vanes, the losses in thrust and mass flow rate, the deflection of the jet plume, and the resulting changes in turbulent kinetic energy k.

The airfoil cross section of the vane plays a significant role on the aerodynamic efficiency of the fan-flow deflection scheme. Symmetric and moderately cambered airfoils (NACA0012 and NACA4412, respectively) provide sufficient deflection at modest losses. Highly cambered airfoils, such as the NACA7514, are very effective in turning the flow but cause serious losses due to shock-wave formation over the vane. The effects of high camber are aggravated when two pairs of vanes are placed relatively close azimuthally. Configurations with the vanes at azimuthal locations substantially off the horizontal plane reduce the overall downward deflection of the plume.

Investigation of the jet plume shows that an overall fan-flow deflection angle of 1.2 deg causes a reduction of about 50% in the peak downward turbulent kinetic energy. Through models proposed in previous studies, this reduction is associated with a suppression of around 4 dB in the peak level of the overall sound pressure level. The relation between plume deflection and reduction in turbulent kinetic energy appears universal for all the nozzle configurations examined here.

With symmetric or moderately cambered airfoils producing a plume deflection angle of 1.2 deg, the specific thrust loss is predicted to be around 0.1%. This loss may be small enough to be tolerated for the entire mission of the aircraft, obviating the complexity of actuating or stowing the vanes. Contributing to the aerodynamic efficiency of the vanes is a pressure redistribution on the core cowl, which results in a small but important increment of positive thrust.

Acknowledgments

The support by NASA Cooperative Agreement NNX07AC62A, monitored by K. B. M. Q. Zaman, is gratefully acknowledged.

References

[1] Brown, C., Bridges, J., and Henderson, B., "Offset Stream Technology Test—Summary of Results," 13th AIAA/CEAS Aeroacoustics Conference, Rome, AIAA Paper 2007-3664, May 2007.

[2] Papamoschou, D., and Nielsen, P., "Fan Flow Deflection for Supersonic Turbofan Engines," 46th AIAA Aerospace Sciences Meeting and Exhibit, Reno, NV, AIAA Paper 2008-0039, Jan. 2008.

[3] Xiong, J., Nielsen, P., Liu, F., and Papamoschou, D., "Computation of High-Speed Coaxial Jets with Fan Flow Deflection," *AIAA Journal*, Vol. 48, No. 10, 2010, pp. 2249–2262. doi:10.2514/1.J050331

[4] Lilley, G. M., "The Source of Aerodynamic Noise," *International Journal of Aeroacoustics*, Vol. 2, Nos. 3–4, 2003, pp. 241–255. doi:10.1260/147547203322986133

[5] Morris, P. J., and Farassat, F., "Acoustic Analogy and Alternative

Theories for Jet Noise Prediction," *AIAA Journal*, Vol. 40, No. 4, 2002, pp. 671–680.
doi:10.2514/2.1699

[6] Bridges, J., Wernet, M., and Brown, C., "Control of Jet Noise Through Mixing Enhancement," NASA TM 2003-212335, June 2003.

[7] Papamoschou, D., and Liu, F., "Aerodynamics of Fan Flow Deflectors for Jet Noise Suppression," *Journal of Propulsion and Power*, Vol. 24, No. 3, 2008, pp. 437–445.
doi:10.2514/1.33415

[8] Dippold, V., Foster, L., and Wiese, M., "Computational Analyses of Offset Stream Nozzles for Noise Reduction," *Journal of Propulsion and Power*, Vol. 25, No. 1, 2009, pp. 204–217.
doi:10.2514/1.34943

[9] Jameson, A., Schmift, W., and Turkel, E., "Numerical Solution of the Euler Equations by Finite Volume Methods Using Runge Kutta Time Stepping Schemes," 14th Fluid and Plasma Dynamics Conference, Palo Alto, CA, AIAA Paper 1981-1259, June 1981.

[10] Menter, F., "Two-Equation Eddy-Viscosity Turbulence Models for Engineering Applications," *AIAA Journal*, Vol. 32, No. 8, 1994, pp. 1598–1605.
doi:10.2514/3.12149

[11] Turkel, E., "A Review of Preconditioning Methods for Fluid Dynamics," *Applied Numerical Mathematics*, Vol. 12, No. 1, 1993, pp. 257–284.
doi:10.1016/0168-9274(93)90122-8

[12] Bohbot, J., Grondin, D., and Darracq, D., "A Parallel/Multigrid Conservative Patched/Sliding Mesh Algorithm for Turbulent Flow," 39th Aerospace Sciences Meeting and Exhibit, Reno, NV, AIAA Paper 2001-1006, Jan. 2001.

J. Powers
Associate Editor